

InsTaG: Learning Personalized 3D Talking Head from Few-Second Video

Jiahe Li¹ Jiawei Zhang¹ Xiao Bai^{1*} Jin Zheng¹ Jun Zhou² Lin Gu^{3,4}

¹School of Computer Science and Engineering, State Key Laboratory of Complex & Critical Software Environment, Jiangxi Research Institute, Beihang University

²School of Information and Communication Technology, Griffith University

³RIKEN AIP ⁴The University of Tokyo

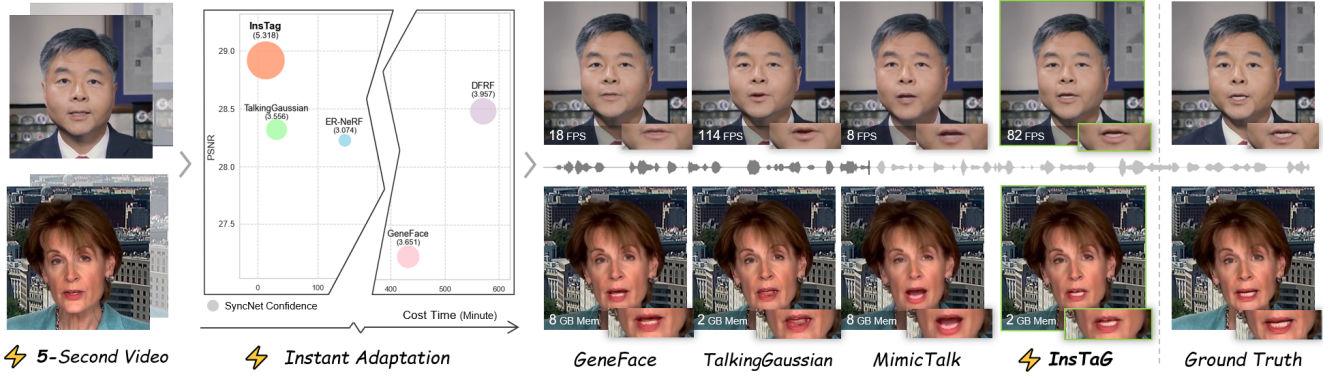


Figure 1. With only 5-second video data, InsTaG outperforms the state-of-the-arts [33, 59, 60] by delivering high-quality personalized lip synchronization and realistic rendering with the fastest adaptation, meanwhile attaining low memory overhead and real-time inference.

Abstract

Despite exhibiting impressive performance in synthesizing lifelike personalized 3D talking heads, prevailing methods based on radiance fields suffer from high demands for training data and time for each new identity. This paper introduces InsTaG, a 3D talking head synthesis framework that allows a fast learning of realistic personalized 3D talking head from few training data. Built upon a lightweight 3DGS person-specific synthesizer with universal motion priors, InsTaG achieves high-quality and fast adaptation while preserving high-level personalization and efficiency. As preparation, we first propose an Identity-Free Pre-training strategy that enables the pre-training of the person-specific model and encourages the collection of universal motion priors from long-video data corpus. To fully exploit the universal motion priors to learn an unseen new identity, we then present a Motion-Aligned Adaptation strategy to adaptively align the target head to the pre-trained field, and constrain a robust dynamic head structure under few training data. Experiments demonstrate our outstanding performance and efficiency under various data scenarios to render high-quality personalized talking heads. Project page: <https://fictionarry.github.io/InsTaG/>.

1. Introduction

Audio-driven talking head synthesis has become an important technique for various digital applications like video production, virtual reality, and human-computer interaction. The recent advancements in Neural Radiance Fields (NeRF) [41] and 3D Gaussian Splatting (3DGS) [26] have led to significant progress in 3D representations. Various methods [19, 32, 33, 37, 47, 59] now utilize radiance fields to create high-fidelity 3D talking head videos, capturing personalized talking styles with impressive photorealistic image quality.

Most of these methods adopt person-specific training. Given a video clip with the target talking person, a whole person-specific model is trained to memorize the target talking head. Despite their tremendous improvements in high-fidelity rendering, personalized dynamics, and fast running speed, as a trade-off, the model holds no generalizability for an unseen identity. Thus, they require a large amount of high-quality video frames with a long training time to adapt to each new identity. Some image-referred methods [36, 47, 60, 61] can quickly generalize to different identities, nevertheless, the quality of personalization and efficiency drop. A question is then raised: *How can we use*

*Corresponding author: Xiao Bai (baixiao@buaa.edu.cn).

the least training data to rapidly learn a faithful 3D talking head, while preserving a high level of personalization?

Observing previous radiance-field-based methods, we notice that: **1)** While the training process includes a long time to learn a basic audio-driven motion that with only little personalized style, the static 3D head can be well reconstructed in just a few early iterations; **2)** Though the results may exhibit jittering and poor quality when trained with limited data, a portion of the lip motions remains recognizable with distinct personalized style. These suggest that even a short video clip can provide rich personalization cues to enable the learning of a specific talking head with little time cost, as long as common audio-motion knowledge is obtained. Motivated by this, by preparing a pre-trained identity-free 3D motion field as prior and aligning it to the new identity to facilitate the adaptation, we propose Instant Talking Head Synthesis with Gaussian Splatting (**InsTaG**), a framework that allows fast learning of high-fidelity personalized 3D talking head from a video even as short as only a few seconds while attaining high efficiency.

Different from previous few-shot methods [36, 60, 61] that imitate a new identity from inputs, InsTaG memorizes the whole talking head in a lightweight person-specific model to obtain high-level personalization and efficiency. Upon such a person-specific paradigm, we fully decouple the learning of universal motion and personalization into pre-training and adaptation, preparing a pre-trained 3D motion field for future person-specific learning of new identity. However, a challenge with this design lies in pre-training with multi-person data, where the person-specific model can not fit varying identities and estimate their varied personalized motions, leading to an ineffective optimization. To tackle this problem, we present an *Identity-Free Pre-training* strategy. By keeping a series of temporary personal fields to store the identity information and filter out the personalized motions, we extract the common knowledge of talking motion from long-video corpus and produce a universal motion field that contains identity-free motion prior. To further facilitate this motion detachment, a negative contrast loss is introduced to encourage the diversity of learned personalized motion between each sample, maximizing the retaining of universal priors for later adaptation.

To fully exploit the universal motion priors to enable fast and high-quality new-identity adaptation, we present a *Motion-Aligned Adaptation* strategy to align the unseen talking head to the pre-trained motion field. First, a motion aligner is developed to learn a condition-independent primitive-wise coordinate offset and a motion scaler. It helps the intra-alignment between the personalized and universal motions in the field, maximizing the retention of learned knowledge during few-shot fine-tuning. Moreover, to enhance the generalizability by face-mouth decomposition [66] while preserving a robust dynamic face structure,

we introduce a face-mouth hook technique to inter-align the inside mouth motion with the face, which efficiently improves the fidelity as well as motion quality. To further improve the robustness of view direction, the new identity’s head structure is aligned with estimated geometry priors for regularization. By incorporating the alignments in the adaptation, the person-specific model finally synthesizes high-fidelity personalized 3D talking heads at a fast speed.

Integrating the two proposed strategies, InsTaG can learn a personalized 3D talking head from even a short 5-second video, achieving state-of-the-art visual quality and personalization compared to existing methods, with high lip-synchronization and real-time inference. Experiments demonstrate the outperforming efficiency and generalizability of InsTaG for various identities, genders and languages.

Our main contributions are summarized as follows:

- An *Identity-Free Pre-training* strategy that enables the pretraining of the person-specific model by filtering out conflict identity and personalized motions, meanwhile maximizing the capturing of universal motion priors.
- A *Motion-Aligned Adaptation* strategy, which inter- and intra-aligns the talking head with the motion field for efficient new-identity adaptation, attaining robust, realistic reconstruction and personalized lip-synchronization.
- Extensive experiments show that our InsTaG learns realistic personalized talking heads from few data, while attaining high lip-synchronization and efficiency, outperforming state-of-the-art methods under various scenarios.

2. Related Work

3D Talking Head Synthesis. Talking head synthesis aims to use arbitrary audio to reenact a talking person to generate audio-visual synchronized videos. Early works [8, 14, 25, 45, 52, 54, 71] are mainly built on generative models, creating talking heads by manipulating the given 2D images. Later, to solve the temporal inconsistency when the head moves, 3D-based methods [39, 51, 62, 68] utilize explicit 3D face structure and successfully improve the naturalness.

Recently, radiance fields like NeRF [41] and 3D Gaussian Splatting (3DGS) [26] have been introduced as the representation to allow 3D talking head synthesis. Inheriting the radiance field optimization, most methods [10, 19, 30, 33, 37, 44, 49] train a person-specific model on minutes of high-quality video, achieving success in reconstructing photorealistic rendering and personalized talking style. However, the strict quality requirements of the training video data and the long training time for every adaptation to a new identity have hugely limited their application. Although some works [36, 47, 59–61, 64] attempt to solve the problem by a one-shot generator [36, 60, 61] or take pre-trained motions from external modules to loosely join the adaptation [47, 59] to achieve one- or few-shot, they often compromise image quality and loses the personalization as the

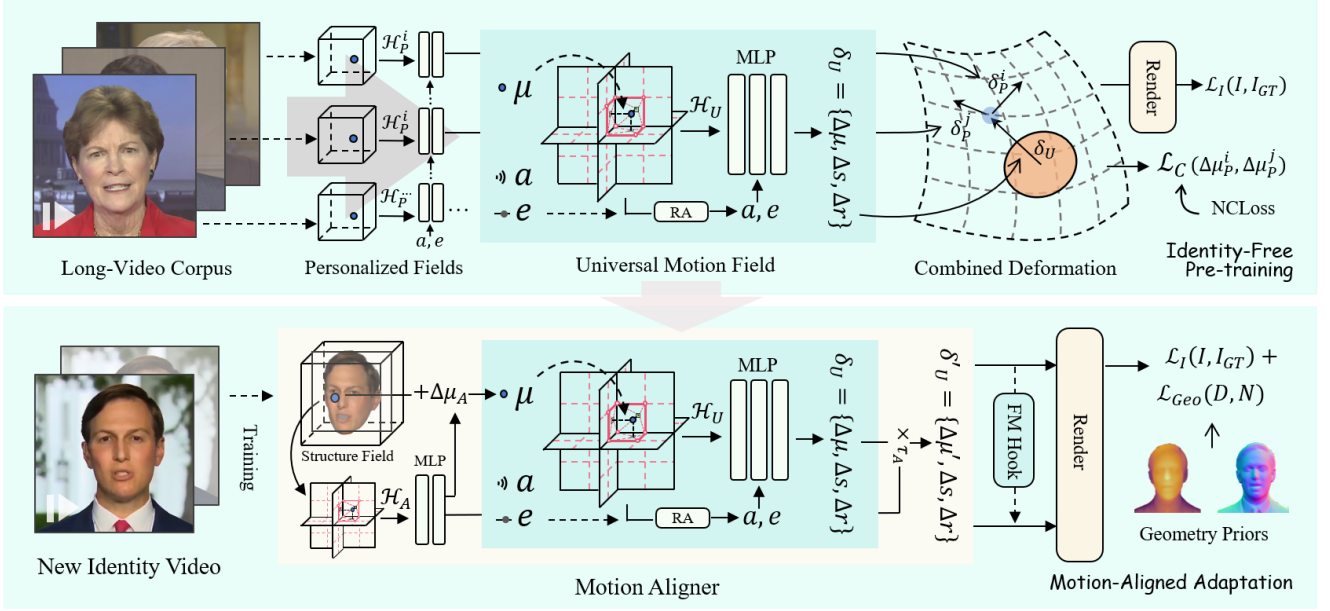


Figure 2. **Overview of InsTaG.** For preparation, InsTaG collects the common knowledge of talking motion from a long-video corpus by *Identity-Free Pre-training*, storing it as a motion field. Given a short video with a new identity, the *Motion-Aligned Adaptation* strategy builds a robust and fast person-specific synthesizer with the pre-trained motion field to learn a high-quality personalized 3D talking head.

trade-off. A concurrent work MimicTalk [60] injects LoRA [24] to improve fine-tuning efficiency, but its inference is slow due to the large backbone. Instead, by enabling the pretraining of person-specific models and using pre-trained motion field to directly drive the talking head, our method obtains a more compact and consistent architecture to fully exploit the motion priors in an end-to-end way, facilitating modeling precise lip-synchronization with high efficiency.

Few-shot 3D Head Reconstruction. Fitting high-fidelity 3D human heads from RGB images has been a hot topic. Early model-based methods [17, 50, 57, 65] focus on fitting a 3D head with 3DMMs [4, 34, 43] but are short in detail. Combined with neural fields, some model-free methods [5, 40, 46] learn static heads from a few images with structure priors. Although many works [6, 15, 18, 22, 48, 56, 58] attempt to reconstruct dynamic heads from few videos, their parametric controls are difficult to predict from audio and limit the mouth motion granularity, making it hard for them to express the highly personalized 3D talking head with delicate audio-driven mouth motions achieved by InsTaG.

Some generative methods [16, 20, 36, 55, 61, 67] focus on reconstructing talking heads with 3D structure, however, they can hardly infer personalized talking style from only one image, leading to weak personalization and fidelity. Learning 3D talking heads with few-shot NeRF, recent works [29, 47, 60] introduce 2D-to-3D modules with pre-training but are often slow due to their overhead. Instead, with an identity-free motion prior and person-specific adaptation instead of expensive 2D-to-3D priors, our InsTaG can rapidly learn a personalized audio-driven 3D talk-

ing head from few data while attaining fast inference.

3. InsTaG

As shown in Figure 2, InsTaG synthesizes personalized 3D talking head based on Gaussian Splatting [26] (Sec. 3.1), consisting of an Identity-Free Pre-training (Sec. 3.2) strategy to fetch universal motion priors and a Motion-Aligned Adaptation strategy (Sec. 3.3) to learn a new identity. We describe the detailed designs in the following sections.

3.1. 3DGS Talking Head Synthesizer

Our framework aims to learn personalized 3D talking head with fast inference and instant adaptation, therefore, a lightweight model with high representation ability is needed to be as the 3D synthesizer. Generally, existing methods can be categorized into image-based [36, 60, 61] and person-specific [19, 30, 33, 49]. The former often possesses generalizability but is relatively slow and weak in personalization, while the latter matches our requirements.

Preliminaries. A person-specific synthesizer based on radiance fields can be formulated as a mapping \mathcal{F} that from given conditions to a synthesized head image I :

$$\mathcal{F} : (\mathbf{a}, \mathbf{e}, [R, t]; \theta) \rightarrow I \quad (1)$$

where the conditions include audio \mathbf{a} , upper-face expression control \mathbf{e} and camera pose $[R, t]$ that represents the head pose, and the parameters of the radiance fields θ .

Under such an architecture, we require the motion learning to be entirely irrelevant to appearance for pre-training. Hence, we leverage the recent 3DGS-based synthesizer with

a face-mouth decomposition [33], including a pair of structure fields and motion fields separately for a face branch and inside-mouth branch to synthesize the talking head image I .

Structure Field. The structure field stores the static Gaussian primitives with parameters $\theta = \{\mu, s, q, \alpha, f\}$. Both the face branch and inside-mouth branch obtain a private structure field for their own target structure.

Motion Field. The motion field predicts a point-wise deformation $\delta = \{\Delta\mu, \Delta s, \Delta q\}$ with a tri-plane hash encoder \mathcal{H} [30] with a region attention (RA) module to store spatial relation, and an MLP decoder to predict deformation. For each query primitive with center μ , the neural field \mathcal{D} predicts its deformation δ from the given condition feature set \mathbf{C} including audio \mathbf{a} and upper-face expression signal \mathbf{e} :

$$\delta = \mathcal{D}(\mu, \mathbf{C}) = \text{MLP}(\mathcal{H}(\mu) \oplus \mathbf{C}), \quad (2)$$

where \oplus denotes concatenation.

Rendering. During rendering, the motion field deforms the Gaussians θ depending on the inputs \mathbf{a} and \mathbf{e} , and then a 2D image is rendered. This process happens in both the face and inside-mouth branches, and the output results are combined to get the final talking head image.

In the following, unless necessary, we do not show the face-mouth decomposition for easier understanding.

3.2. Identity-Free Pre-training

Although with personalization knowledge, a short video clip is insufficient to train a talking head with personalized audio-motion mapping from scratch. To this end, we extract the common motion knowledge from long videos by pre-training as compensation for the new identity.

In contrast to existing generative pre-training solutions [36, 47, 60] that allow multiple-identity inputs to train the same model, an identity-conflict problem lies in our method. Firstly, different identities can not coexist in one person-specific model. Secondly, since the model can not separate different people, the conflicting personalized motion hinders the model convergence and pollutes the pre-trained module by overfitting the noises.

Strategy. To tackle this problem, we design storing the identity-dependent knowledge in a *Personalized Field* distributed to each training video, therefore detaching the identity influence of the learning of universal motion to pre-train a *Universal Motion Field*. Specifically, each Personalized Field consists of a personalized structure field with parameter θ_P and a smaller motion field \mathcal{D}_P to retain the identity appearance and personalized motion of its owner video.

Universal Motion Field (UMF). Serving as a pre-trained module, UMF aims to predict a commonly correct facial motion that suits most identities. Queried by an arbitrary Gaussian, the field \mathcal{U} predicts the universal deformation δ_U without personalization according to Eq. (2):

$$\delta_U = \mathcal{U}(\mu, \mathbf{C}) = \text{MLP}(\mathcal{H}_U(\mu) \oplus \mathbf{C}). \quad (3)$$

Personalized Fields. During training, Personalized Fields cooperate with one sharing Universal Motion Field to synthesize personalized talking heads, enabling the supervision from videos with different identities. Practically, given an audio feature \mathbf{a} and expression signal \mathbf{e} packaged by \mathbf{C} , the UMF \mathcal{U} would predict an identity-free deformation queried by $\mu_P^i \in \theta_P^i$, serving as a basic deformation for the i -th person. Meanwhile, the i -th personalized field predicts a residual motion δ_P^i as the personalized adjustment:

$$\delta_P^i = \mathcal{D}_P^i(\mu_P^i, \mathbf{C}) = \text{MLP}(\mathcal{H}_P^i(\mu_P^i) \oplus \mathbf{C}). \quad (4)$$

After that, the two deformations are combined to deform the personalized structure fields for rendering:

$$\mathcal{R} : ([R, t], \tilde{\theta}_P^i) \rightarrow I, \quad \tilde{\theta}_P^i = \theta_P^i + \delta_U + \delta_P^i, \quad (5)$$

where \mathcal{R} refers to the 3DGS rendering process.

Since then, videos with different talking identities can be used for pre-training with no identity conflicts, and the personalized motions are isolated from each other by staying at the personalized fields, detached from the universal ones.

Negative Contrast Loss. Despite the detachment of personalized and universal motions enabled, a new problem emerges: how to decide whether a motion should be personalized or universal? Without supervision, a native separation from gradient would be highly biased because of uncertainties like initialization and data disparity, making some personalized motions inappropriately stored into the universal field but too much universal knowledge omitted.

For this problem, we introduce a Negative Contrast Loss with two principles: 1) the ideal personalized motions are expected to be the minimum additional motions that enable smooth model convergence, thus the fewer the better; 2) subject to the first point, the personalized motions of one identity should be different from that of the others. Therefore, we design the loss by a truncated dot product:

$$\mathcal{L}_C(\Delta\mu_P^i, \Delta\mu_P^j) = \mathbb{I}_{trunc}(\Delta\mu_P^i \cdot \Delta\mu_P^j), \quad (6)$$

where $(\Delta\mu_P^i, \Delta\mu_P^j)$ is a pair of personalized μ -deformation from i -th and j -th personalized fields, queried by the same μ_P and \mathbf{C} in Eq. (4), and \mathbb{I}_{trunc} is a truncation function:

$$\mathbb{I}_{trunc}(x) = \begin{cases} x, & x > 0 \\ 0, & x \leq 0 \end{cases}. \quad (7)$$

This negative-sample-based contrastive loss works from two aspects: 1) when the two participants are close in the 3D space, the loss would encourage them to be either different in direction or less in effect; 2) if the participants are already significantly different, or if one of the participants is close to 0, the loss stops pushing them too far.

By contrasting the negative personalized $\Delta\mu$ pairs, the proposed loss can encourage learned personalized motion to be diverse between the different personalized fields, therefore maximizing the filtering to get universal motions.

3.3. Motion-Aligned Adaptation

Based on the pre-trained UMF from Sec. 3.2, we introduce a *Motion-Aligned Adaptation* strategy to allow fast and high-quality learning of new-identity talking heads from a short video. Different from existing works [36, 47, 60] that take motions to guide image generation, we directly drive Gaussians by deformation in the final rendering for more realistic visual quality, bringing a challenge in precisely aligning the pre-trained motion to the new identity’s head.

Motion Aligner. Due to the diversity of human faces, the pre-trained UMF can not natively match all unseen identities suitably. Except for the personalization that we aim to learn, this motion misalignment exists in two aspects: 1) the target facial structure may be biased with the implicit one from pre-training in UMF; 2) the motion of the target identity may have a scale gap from the universal motion.

To this end, we propose to wrap a Motion Aligner on the motion field to learn the adjustment. Specifically, a multi-resolution positional encoder \mathcal{H}_A is first added to store the spatial information. Then, before querying the motion field by μ from the structure field, a coordinate offset $\Delta\mu_A$ is predicted as bias adjustment:

$$\Delta\mu_A = \text{MLP}(\mathcal{H}_A(\mu)) \in \mathbb{R}^3. \quad (8)$$

After getting the universal deformation δ_U , the $\Delta\mu$ part is multiplied by a scaling factor $\tau_A \in \mathbb{R}^3$ predicted in the same way as Eq. (8) for scale alignment, and finally output the adjusted deformation $\delta'_U = \{\Delta\mu', \Delta s, \Delta q\}$, where

$$\Delta\mu' = \Delta\mu \times \tau_A, \quad \Delta\mu \in \mathcal{U}(\mu + \Delta\mu_A, \mathbf{C}). \quad (9)$$

Here δ'_U is used as the final deformation for rendering.

Face-Mouth Hook. As a deformation-based framework, the asynchronous inside and out mouth motions often deteriorate the modeling [33]. As in Sec. 3.1, we adopt a face-mouth decomposition [33] to solve this problem. It separates the modeling of the face (including lips) and inside of the mouth into two branches. However, when data is reduced, these two parts may fail to learn to move in harmony, causing misalignment with low visual quality. Without an existing mechanism to ensure the inter-alignment, we suggest setting a hook in the motion field to allow the mouth to actively align to the face, as shown in Figure 3.

Given a predicted deformation δ_F from the face branch that represents face motion, we attempt to fetch the motions on lips from it to guide the inside-mouth deformation δ_M . Considering the lip motion tends to cause the largest deformation amount of the whole face, we take the maximal and minimal $\Delta\mu^F \in \delta_F$ (denoted as $\Delta\mu_{\max/\min}$) as the motion cues, and calculate a distance $\mu_{\text{dist}} = \Delta\mu_{\max} - \Delta\mu_{\min}$ for a direct scale cue. Then, this set of features $\varphi = \{\Delta\mu_{\max}, \Delta\mu_{\min}, \mu_{\text{dist}}\}$ are input in the MLP decoder in the inside-mouth branch motion field to predict a deforma-

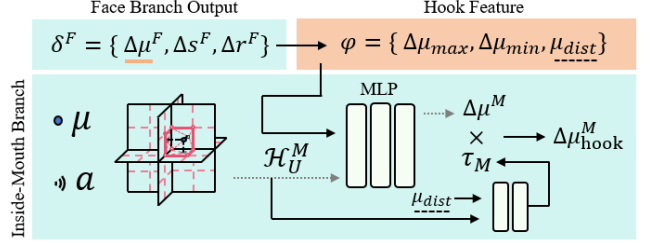


Figure 3. **Illustration of Face-Mouth Hook.** We hook the motion of the mouth to the generated face motion, allowing an alignment across two branches to enhance robustness under few training data.

tion $\Delta\mu$. The mouth motion field can be formulated as:

$$\Delta\mu^M = \mathcal{U}^M(\mu, \{\mathbf{a}, \varphi\}). \quad (10)$$

Representing a structure difference, \mathcal{U}^M does not take e as input and does not predict deformations on r and s .

Moreover, considering the opening degree of the inside mouth should align with that of the lips, we hook the motion scaling prediction to the facial motion scale cue μ_{dist} . To achieve this, a scaling factor τ_M is predicted for each μ by an MLP to get the final primitive-wise deformation:

$$\mu_{\text{hook}}^M = \Delta\mu^M \times \tau_M, \quad \tau_M = \text{MLP}(\mathcal{H}_U^M(\mu) \oplus \mu_{\text{dist}}), \quad (11)$$

where \mathcal{H}_U^M is the \mathcal{H} of the UMF in the inside-mouth branch.

This hook technique establishes a connection between the motion fields to guide the mouth motion to align to the face, while the former’s scale is also explicitly connected to the latter, bringing robust performance on the face-mouth alignment even when with only few training data.

Geometry Prior Regularizer. To further reduce the geometry ambiguity caused by the lack of view cover, we leverage the power of advanced human geometry estimator [27] to provide extra geometry cues for regularization. To solve the geometry degradation [31] and instability of 3DGS at unseen views [9], we add two regularizers on the depth and surface normal. Following [9] we first calculate the 2D depth D and normal N_s when synthesizing image I . Then, the estimated monocular depth map \tilde{D} and normal \tilde{N} from the ground-truth image are used for regularization:

$$\mathcal{L}_{Geo} = \lambda_D L_D(D, \tilde{D}) + \lambda_N \sum_{i=0}^m \sum_{j=0}^n (1 - N_{i,j} \cdot \tilde{N}_{i,j}), \quad (12)$$

where L_D is a scale-invariant depth loss, $N_{i,j}$ denotes the normal at pixel (i, j) , and (m, n) is the shape of image I .

3.4. Training Details

Photometric Loss. The training processes are mainly supervised by the image photometric loss \mathcal{L}_I between the synthesized image I and its ground-truth I_{GT} . Following 3DGS [26], \mathcal{L}_I consists of an L1 and a D-SSIM [53] terms.

Pre-training. During pre-training, we collect k videos as training data to simultaneously train the UMF. For each syn-

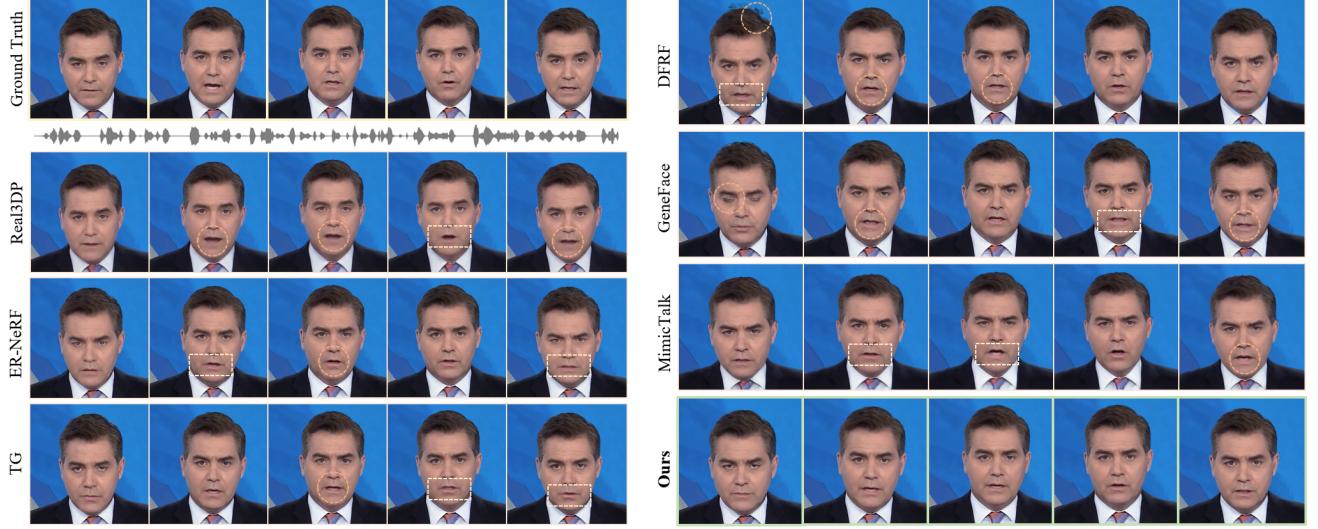


Figure 4. **Qualitative Comparison on Synchronization.** Our method performs best in both lip-synchronization and visual quality. “Real3DP” and “TG” denote [61] and [33]. Better visualized with **zoom-in**. We recommend watching the *supplementary video*.

Methods	Setting	Rendering Quality			Motion Quality			Efficiency		Real-time
		PSNR (A/F) ↑	LPIPS (A/F) ↓	SSIM ↑	LMD ↓	AUE-(L/U) ↓	Sync-C ↑	Training ↓	FPS ↑	
Ground Truth		N/A	0 / 0	1.000	0	0 / 0	8.897	-	-	
EAT [16]	One-shot	- / 22.44	- / 0.060	0.712	-	1.309 / 1.011	7.577	-	11.8	✗
Real3DPortrait [61]		23.58* / 25.37	0.104* / 0.054	0.821	<u>3.407</u>	1.148 / 1.098	<u>7.549</u>	-	8.4	✗
RAD-NeRF [49]	Trained From Scratch	28.36 / 25.51	0.048 / 0.035	0.835	3.555	1.295 / 0.732	2.249	5 hours	28.6	✓
ER-NeRF [30]		28.23 / 25.63	<u>0.040</u> / 0.031	0.844	3.541	1.327 / 0.451	3.074	2 hours	30.8	✓
GaussianTalker [10]		28.18 / 25.61	0.043 / 0.032	0.836	3.647	1.379 / 0.415	1.970	67 min	64.5	✓
TalkingGaussian [33]		28.32 / 26.01	0.041 / <u>0.028</u>	0.843	3.588	1.158 / <u>0.316</u>	3.556	31 min	114.2	✓
DFRF [47]	Adaptation & Few-shot	<u>28.48</u> / <u>26.26</u>	0.066 / 0.034	<u>0.859</u>	3.436	1.247 / 0.683	3.957	9 hours	0.03	✗
GeneFace [59]		27.23 / 25.08	0.052 / 0.036	0.823	3.510	1.310 / 0.684	3.651	7 hours	18.1	✗
MimicTalk [60]		24.69* / 26.27	0.075* / 0.031	0.853	3.489	<u>0.958</u> / 0.775	6.926	<u>16 min</u>	8.2	✗
InsTaG (Ours)		28.86 / 26.32	0.039 / 0.026	0.861	3.167	0.926 / 0.313	5.318	13 min	<u>82.5</u>	✓

Table 1. **Quantitative Comparison in self-reconstruction setting** with 5s training data. InsTaG achieves the best image quality and personalized dynamics, with fast adaption and real-time inference. We mark the **best** and second-best results. (*: with synthesized torso.)

thesized image I^i from i -th video, we first calculate its photometric loss, and then calculate the Negative Contrast Loss to each other. The pre-training loss for the i -th video is:

$$\mathcal{L}_{pre}^i = \mathcal{L}_I(I^i, I_{GT}^i) + \lambda_C \sum_{j=1, j \neq i}^k \mathcal{L}_C(\Delta \mu_P^i \cdot \Delta \mu_P^j). \quad (13)$$

Adaptation. For adaptation, we initialize a person-specific model with the pre-trained UMF. A warm-up stage first runs without a Motion Aligner and geometry loss for a start. After that, the model is trained with full loss:

$$\mathcal{L}_{ada} = \mathcal{L}_I(I, I_{GT}) + \mathcal{L}_{Geo}(D, N). \quad (14)$$

4. Experiments

Dataset. In the experiments, we collect a long-video corpus with 5 long speaking videos from [30, 59] for pre-training, and follow prevailing settings [19, 30, 33, 59] to take 4 videos from publicly-released sets [47, 59] for the test, with no identity overlap of the two parts. The videos have an average length of about 800-8000 frames in 25 FPS with a

center portrait, all are cropped and resized to 512×512 .

Implementation Details. Our method is implemented on PyTorch. The pre-training stage lasts 150,000 iterations and adaptation lasts 10,000. An AdamW [38] optimizer is used with learning rates of $5e-3$ and $5e-4$ separately for the grid and neural networks to train UMF. λ_D , λ_N and λ_C are set to $1e-2$, $1e-3$ and 1. All experiments are performed on RTX 3080 Ti GPUs. The overall pre-training takes about 5 hours. The head pose is estimated through BFM [43]. A DeepSpeech model [21] is used to extract basic audio features following previous works [19, 30, 33].

Comparison Baselines. To compare with the state-of-the-art methods, we take the baselines from the relevant person-specific methods DFRF [47], RAD-NeRF [49], GeneFace [59], ER-NeRF [30], TalkingGaussian [66], GaussianTalker [10] and a concurrent method MimicTalk [60]. We also involve the one-shot EAT [16] and Real3DPortrait [61]. All the methods are reproduced by their official codebase. If officially supported, we use DeepSpeech as audio extactor.

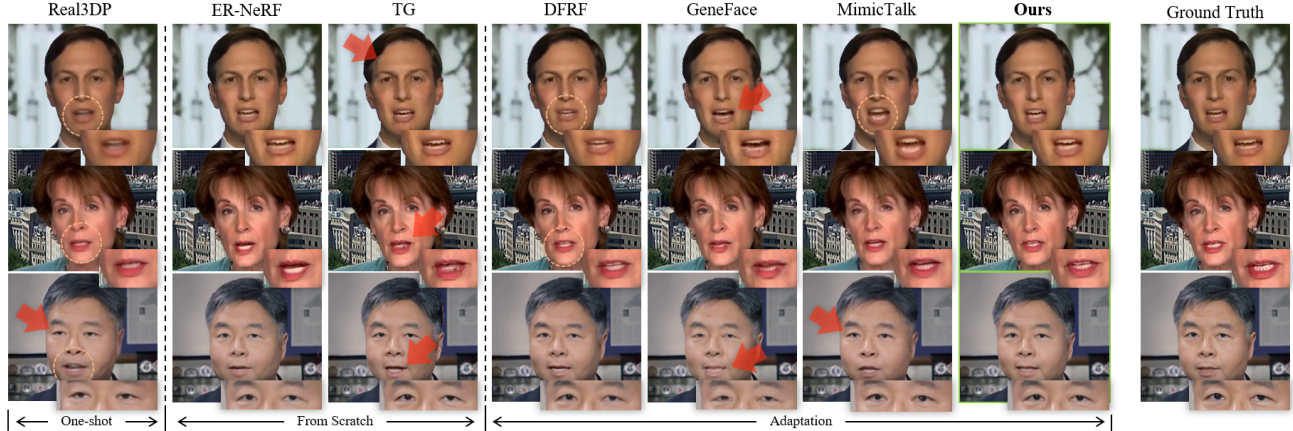


Figure 5. **Qualitative Comparison on Reconstruction Quality.** Our method performs the best in rendering photorealistic talking heads with fine details. “Real3DP” and “TG” denote Real3DPortrait [61] and TalkingGaussian [33]. Better visualized with **zoom-in**.

Method	Type	5s			10s			20s		
		PSNR \uparrow	AUE-L \downarrow	Sync \uparrow	PSNR \uparrow	AUE-L \downarrow	Sync \uparrow	PSNR \uparrow	AUE-L \downarrow	Sync \uparrow
ER-NeRF [30]	From Scratch	28.235	1.327	3.074	28.728	1.078	3.240	29.287	<u>0.941</u>	4.638
TalkingGaussian [33]		28.321	<u>1.158</u>	3.556	<u>29.130</u>	1.069	4.663	<u>29.536</u>	<u>1.073</u>	<u>4.776</u>
DFRF [47]	Adaptation	<u>28.481</u>	1.247	<u>3.957</u>	28.881	1.072	4.210	29.253	1.137	4.333
GeneFace [59]		28.227	1.310	3.651	27.997	<u>1.036</u>	<u>4.869</u>	28.825	1.033	4.772
InsTaG (Ours)		28.863	0.926	5.318	29.421	0.881	5.636	30.352	0.710	5.764

Table 2. **Quantitative Comparison in self-reconstruction setting** to person-specific baselines with different data amounts. Our method performs best in various data scenarios, exhibiting robustness. The best and second-best results are in **bold** and underline.

Methods	Audio <i>English, Male</i>		Audio <i>German, Female</i>	
	Sync-E \downarrow	Sync-C \uparrow	Sync-E \downarrow	Sync-C \uparrow
Full Baseline [33]	10.443	4.342	9.942	4.949
ER-NeRF [30]	11.711	3.043	11.502	2.853
TalkingGaussian [33]	10.675	4.317	10.898	3.708
DFRF [47]	10.515	4.726	<u>10.482</u>	<u>4.329</u>
GeneFace [59]	<u>9.995</u>	<u>4.734</u>	11.029	4.162
InsTaG (Ours)	9.886	4.828	9.733	4.990

Table 3. **Comparison in cross-domain setting** with 20s training data. We take TalkingGaussian [33] with full data for reference.

4.1. Evaluation

Comparison Settings. The quantitative comparison contains two settings: **1)** The *self-reconstruction setting*. In this setting, we split each of the 4 adaptation videos into several few-second training sets and a test set of at least 12s, and use the unseen test data as input and ground truth for evaluation. **2)** The *cross-domain setting*, where we use an unseen English male audio from NVP [51] and a German female one from [19] to test the cross-domain generalizability. To fully evaluate the baselines with failure models, we use 20s from the only English female video to train one model per method that represents the best performance for testing.

Metrics and Measurements. We employ PSNR, LPIPS [69], and SSIM [53] to evaluate image quality. Especially, we report PSNR and LPIPS separately on an all image (“A”) and only the aligned face (“F”). SSIM is only measured on the face. For lip synchronization, we use LMD [7] and

SyncNet [11, 12] confidence (Sync-C) and error (Sync-E). Besides, action unit [13] error (AUE) is used on upper-face (AUE-U) and lower-face (AUE-L) following [33], in which AUE-L can reflect the similarity of the personalized talking actions from the target. We also statistic the training time (fine-tuning time for few-shot or adaptation-based methods) and inference FPS to evaluate efficiency.

Quantitative Evaluation. **1)** Table 1 reports the results of *self-reconstruction setting* with 5s training data. Our method achieves the best image quality, demonstrating our ability to faithfully generate a realistic talking head. Inheriting the traditions of large corpus pre-training, the one-shot methods [16, 61] and MimicTalk [60] achieve very high Sync scores but are relatively slow. Also getting a high Sync, InsTaG achieves the best in LMD and AUE-L, showing our advantage in preserving personalization. While all baselines can not simultaneously achieve high synchronization and real-time inference, our method produces the best overall performance including the fastest adaptation and high speed. **2)** When data increases, the results in Table 2 show that InsTaG still outperforms other person-specific models in all aspects, demonstrating our wider application value and robustness to various scenarios. **3)** In the results from Table 3 in *cross-domain setting*, where the methods are tested on two difficult cross-domain scenarios, the advantages of pre-training are further amplified. GeneFace [59] and DFRF [47] surpass all models trained from scratch. At the same time, InsTaG exceeds the baseline [33] trained

Methods	ER-NeRF [30]	TalkingGaussian [33]	GaussianTalker [10]	DFRF [47]	GeneFace [59]	MimicTalk [60]	InsTaG (Ours)
Lip-sync Accuracy	2.00	1.90	1.50	3.30	2.70	4.80	4.50
Image Quality	3.40	3.70	4.00	2.90	3.10	3.70	4.80
Identity Preserving	2.40	1.50	1.70	2.90	3.00	<u>4.20</u>	4.60
Video Realness	1.40	1.50	1.40	2.80	1.70	<u>3.20</u>	3.90

Table 4. **User Study.** The rating is in the range of 1-5, higher denotes better. The best and second-best results are in **bold** and underline.

Pre-training		Adaptation		PSNR \uparrow	LPIPS \downarrow	LMD \downarrow	Sync-C \uparrow
PField	NCLoss	Aligner	Hook				
				28.66	0.044	3.734	2.019
\checkmark				28.76	0.040	3.239	4.816
\checkmark	\checkmark			28.59	0.041	<u>3.223</u>	5.124
\checkmark	\checkmark	\checkmark		28.69	<u>0.040</u>	3.274	5.233
\checkmark	\checkmark		\checkmark	28.66	0.040	3.257	5.086
\checkmark	\checkmark	\checkmark	\checkmark	<u>28.79</u>	0.040	3.226	4.994
\checkmark	\checkmark	\checkmark	\checkmark	28.86	0.039	3.167	5.318

Table 5. **Ablation Study.** We verify the components under 5s *self-reconstruction* setting, showing the effect of our contributions.

on about 1-minute full training data, demonstrating the outstanding robustness and generalizability of our method.

Qualitative Evaluation. To qualitatively evaluate the results, we show the generated sequences and rendering details from *self-reconstruction* setting. In Figure 4, it can be observed that the models trained from scratch (ER-NeRF, TG) [32, 33] behave poorly in synchronization (yellow box), while the adaptation-based methods (DFRF, GeneFace, MimicTalk) [47, 59, 60] perform better but generate blurry results (orange circle). Referring to Figure 5, while all methods synthesize either blurs or heavily distorted details (red arrow), our method can reconstruct photorealistic appearance and delicate details. By benefitting from the advantages of both pre-training and person-specific training, InsTaG achieves the best in both synchronization and image quality. We strongly recommend watching our *supplementary video* for an intuitive comparison.

User Study. To better judge the quality in real human-participated scenarios, we conducted a user study with 28 generated talking head videos from 7 methods with 5s training data. We invited 10 attendees to rate each anonymous method from four aspects: (1) Lip-sync Accuracy; (2) Video Realness; (3) Identity Preserving and (4) Video Realness. The results in Table 4 show that our InsTaG achieves the best in three aspects and the second-best in lip-sync, which is only after the concurrent MimicTalk [60], demonstrating our outstanding visual quality via human judgment.

4.2. Ablation Study

We conduct the ablation study to prove the effectiveness of our contributions. The results are reported in Table 5.

Identity-Free Pre-training. In the first row, we show the results pre-trained without Personalized Fields (PField), which produces bad synchronization due to the identity-conflict problem. After applied PField, the pre-training

Backbone	Hook	PSNR \uparrow	LPIPS \downarrow	LMD \downarrow	Sync-C \uparrow
Single Branch	-	28.59	0.049	<u>3.233</u>	4.675
Face-Mouth Decomp.	\times	28.69	0.040	3.274	<u>5.233</u>
Face-Mouth Decomp.	\checkmark	28.86	0.039	3.167	5.318

Table 6. **Ablation Study on Mouth Motion Representation.** Introducing FMD [33] can effectively improve lip-synchronization, while our FM hook technique further boosts image quality.

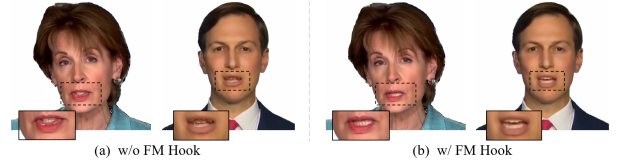


Figure 6. **Visualization Results of Face-Mouth Hook.** FMD improves performance but also causes misalignment when with inadequate data, which can be well solved by our Face-Mouth Hook.

works with obvious effect. Combined with PField, Negative Contrast Loss (NCLoss) shows its impact on lip-sync improvement, offering higher Sync-C. This demonstrates the necessity of PField in enabling the pre-training and the effect of NCLoss on encouraging knowledge collection.

Motion-Aligned Adaptation. We apply our Motion Aligner (Aligner) and Face-Mouth Hook (FM Hook) to illustrate their effect on adaptation. Although the performance is improved by applying our pre-training strategy, the Aligner can bring extra enhancement by providing adaptation adjustments. Furthermore, the Hook works in both visual quality and dynamics by correcting inside-mouth misalignment. Combining these two adaptation techniques, the performance achieves the best among all settings.

Mouth Motion Representation. To further explain the necessity of Face-Mouth Decomposition (FMD) [33] and our FM Hook, we take studies by using one single branch to represent the two parts. Results in Table 6 show the effect of FMD. However, simply introducing it would cause significant misalignment that lowers the visual quality, as in Figure 6. By applying our FM Hook, this drawback can be well solved to benefit FMD with robust performance, generating synchronized talking heads with high visual quality.

5. Ethical Consideration

We hope our method can promote the healthy development of digital industries. However, it is important to note that it could be misused for malicious purposes, potentially causing negative impacts. As part of our responsibility, we will assist in developing deepfake detection tools. We recommend the responsible use of this and all similar techniques.

InsTaG: Learning Personalized 3D Talking Head from Few-Second Video

Supplementary Material

Overview

In the supplementary material, we first report additional experiments in Sec. 6, and describe the details of the dataset and implementation in Sec. 7 and 8. We further show the visualized result in Sec. 9, and discuss the ethical consideration and limitations in Sec. 11 and 12. For a better explanation, a supplementary video is additionally provided.

6. Additional Experiments

6.1. Ablation Study

Personalized Field. To further verify the effect of the Personalized Field in pre-training, we conduct a fine-grained ablation study to separately show the effect of the structure field and motion field in it. The results are reported in Table 7. Due to the identity-conflict problem discussed in Sec. 3.2, it can be observed that the pre-training totally fails in helping adaptation when without the personalized structure field, resulting in very low Sync-C scores. Though a significant performance raise happens after applying structure fields, the image quality and synchronization are still not ideal because the heavily overfitted pre-training model is hard to adjust well during the fine-tuning, resulting in unexpected distortions, as shown in Figure 7. After applying the full Personalized Fields, our method achieves the best performance, demonstrating the effect of the two parts.

Structure	Motion	PSNR \uparrow	LPIPS \downarrow	LMD \downarrow	Sync-C \uparrow
\times	\times	28.67	0.044	3.734	2.019
\times	\checkmark	28.63	0.045	3.715	2.312
\checkmark	\times	28.59	<u>0.040</u>	<u>3.228</u>	<u>4.975</u>
\checkmark	\checkmark	28.86	0.039	3.167	5.318

Table 7. **Ablation Study on Personalized Field.** The best and second-best results are highlighted with **bold** and underline.

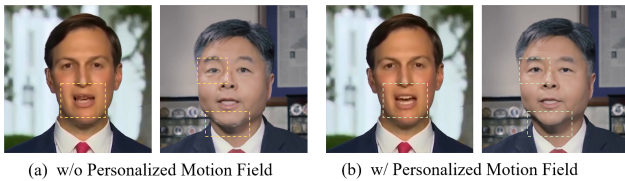


Figure 7. **Visualized Results of Personalized Motion Field.** The overfitting of personalized motions from multiple persons pollutes the pre-trained module and leads to unexpected distortions on new identities, which can be well solved by adding a motion field in the Personalized Field during pre-training.

Motion Aligner. We take an additional ablation study inside the Motion Aligner to illustrate the effect of the two involved alignments. As shown in Table 8, when not applying the offset alignment $\Delta\mu_A$ from Eq. (8), the performances are relatively worse on Sync-C with a lower PSNR. This comes from the insufficient inheritance of the pre-trained knowledge due to the head structure misalignment. After adding the offset adjustment, Sync-C and PSNR increase significantly. Combined with the scale adjustment τ_A from Eq. (9), our method finally achieves an ideal performance.

Offset	Scale	PSNR \uparrow	LPIPS \downarrow	LMD \downarrow	Sync-C \uparrow
\times	\times	28.66	0.040	3.257	5.086
\times	\checkmark	28.68	0.040	3.211	5.113
\checkmark	\times	28.77	<u>0.040</u>	<u>3.192</u>	<u>5.229</u>
\checkmark	\checkmark	28.86	0.039	3.167	5.318

Table 8. **Ablation Study on Motion Aligner.** The best and second-best results are highlighted with **bold** and underline.

Geometry Prior Regularizer. Scenes purely reconstructed by radiance fields have excellent visual quality at interpolated viewpoints. However, they are weak in extrapolation, which corresponds to the situations where the talking heads rotate to an unseen angle during synthesis. One main reason is that the geometry is degraded due to the limited view coverage, as shown in Figure 8. To tackle this problem, we use the Geometry Prior Regularizer to provide extra constraints to help the 3D head reconstruction. Since these troubles often appear only in a few frames and influence slightly on the overall numerical metrics, we reveal them quantitatively to verify the effect of the regularizer. As shown in Figure 9, the regularizer successfully tackles the mist-like artifacts due to an inaccurate surface location, and thus brings better visual quality.

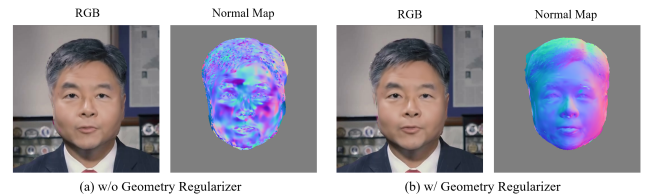


Figure 8. Due to the limited view coverage, the geometry of the 3D talking head degrades, leading to inaccurate surfaces.

6.2. Audio Feature Extractor

In the main paper, we use DeepSpeech [21] as the audio feature extractor to align with most previous works [30, 33, 47]

Methods	Extractor	Rendering Quality			Motion Quality		
		PSNR \uparrow	LPIPS \downarrow	SSIM \uparrow	LMD \downarrow	AUE-(L/U) \downarrow	Sync-C \uparrow
Ground Truth		N/A	0	1.000	0	0 / 0	8.897
RAD-NeRF [49]	Wav2Vec 2.0	27.42	0.050	0.831	3.898	1.437 / 0.879	2.299
ER-NeRF [30]	Wav2Vec 2.0	27.87	0.041	0.848	3.624	1.427 / 0.610	2.856
TalkingGaussian [33]	Wav2Vec 2.0	28.13	0.041	0.850	3.612	1.226 / 0.400	3.635
GeneFace [59]	HuBERT	28.23	0.052	0.823	3.510	1.310 / 0.684	3.651
ER-NeRF [30]	HuBERT	27.56	0.043	0.832	3.827	1.595 / 0.529	1.853
TalkingGaussian [33]	HuBERT	28.23	0.043	0.840	3.860	1.312 / 0.467	3.367
InsTaG (Ours)	DeepSpeech	28.86	0.039	0.861	3.167	0.926 / 0.313	5.318
	HuBERT	29.00	<u>0.040</u>	0.861	3.174	1.031 / <u>0.388</u>	5.239
	Wav2Vec 2.0	<u>28.89</u>	0.041	0.867	3.111	0.924 / 0.463	5.852
TalkingGaussian [33]	AVE	28.52	0.041	0.845	3.075	0.836 / 0.631	8.047
InsTaG (Ours)	AVE	28.83	0.040	0.852	2.984	0.742 / 0.365	7.787

Table 9. **Comparison with Different Audio Feature Extractors** using 5s training video. The best and second-best results are highlighted with **bold** and underline. After applying an advanced extractor, our method gets further improvements, showing the scaling potential.

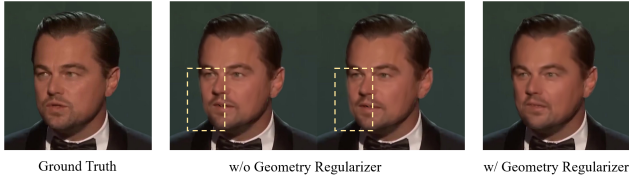


Figure 9. By introducing geometry constraints, our method successfully solves the serious artifacts in difficult unseen views and thus provides a clearer talking head with accurate structure.



Figure 10. **Comparison with AVE audio extractor.** Our InsTaG shows advantage in rendering quality and robustness.

for a fair comparison. Besides, our InsTaG can also apply other advanced audio extractors like in previous radiance-field-based methods to get a performance improvement. As shown in Table 9, when applying Wav2Vec 2.0 [1] and HuBERT [23], our method gains improvements in different aspects. With the help of Wav2Vec, InsTaG achieves a high Sync-C score and better image quality as well compared to DeepSpeech. HuBERT mainly helps in image quality especially on PSNR, while the lip synchronization drops a bit. Interestingly, we observe this phenomenon also appears on other baselines like ER-NeRF and TalkingGaussian. We consider this because its high feature dimension brings extra difficulty in training with few data. While the baselines still fail to produce reasonable results with a short training video, our method performs best in all aspects.

Additionally, we later noticed that the AVE encoder in

Item	Infer.	Adapt.	P-1	P-2	P-3	P-4	P-5
VRAM (MB)	1826	2214	2200	2188	2194	2204	2270

Table 10. **Peak GPU Memory Cost.** P- k denotes the pre-training process with k personalized fields involved. The results show the high efficiency of InsTaG and its huge scaling potential.

SyncTalk [44] may perform a similar effect as our method, which is pre-trained on large corpus with a lip-sync expert discriminator. Therefore, the extracted signal is much suitable for the task of talking head synthesis. Here we add a comparison between TalkingGaussian and our method in Table 9. As shown, AVE can exactly boost the results and achieves an extremely high Sync-C, surpassing even the one-shot methods in Table 1. However, TalkingGaussian fails to produce high-fidelity images. Without a comprehensive 3D motion prior, the rendered images often have heavy noises and the motions are jittering, leading to worse rendering, as visualized in Figure 10. According to the AUE and LMD, it can be observed that the reconstructed talking head is suboptimal with insufficient personalization, while it also can't enable the pre-training of upper-face expressions. While equipped with the stronger AUE, our method can even get a more comprehensive performance, especially in Sync-C that is weak with ASR extractors, surpassing all the baselines in Table 1.

6.3. Efficiency Analysis

Besides the inference FPS and training time, we additionally report the GPU memory cost to show the efficiency of our method. From Table 10, it can be observed that our InsTaG is efficient in all processes including inference (infer.), adaptation (adapt.), and pre-training (P- k) with multiple personalized fields. Notably, since the personalized

Method	Time	PSNR \uparrow	LPIPS \uparrow	LMD \uparrow	Sync-C \uparrow
ER-NeRF	2 hours	30.07	0.0279	3.111	5.088
TalkingGaussian	34 min	31.04	0.0267	3.001	6.005
InsTaG-10K	13 min	31.37	0.0312	2.909	6.005
InsTaG-25K	32 min	31.15	0.0305	2.893	6.143

Table 11. **Comparison with Full Training Data.** We use full of the training data to evaluate the performance. 10K and 25K denote trained with 10,000 and 25,000 iterations.

fields cost only little storage, the GPU memory cost increases slightly along with the number of fields involved. Thus, there is still a huge space to enhance the performance by adding more pre-training data.

6.4. More Training Data

We further evaluate the performance with more training data, which is similar to the setting in previous person-specific methods [19, 30, 33, 49]. As shown in Table 11, InsTaG still outstands by achieving higher lip synchronization in a shorter time. This shows the common knowledge from pre-training can not only work in few-shot settings but also provide a universal improvement for various data scenarios.

6.5. Comparison with DDPM Baselines

Here we add two current SOTA DDPM-based methods MEMO [70] and Ditto [35], which support 512×512 generation, for Table 1’s comparison. Since they can not reenact the head trace, we report the image quality metrics of the aligned face. While these generative models perform worse in personalization (AUE), visual quality, and speed, InsTaG shows superior overall performance with real-time inference capability.

Methods	PSNR \uparrow	LPIPS \downarrow	SSIM \uparrow	LMD \downarrow	AUE-(L/U) \downarrow	Sync-C \uparrow	FPS \uparrow
MEMO	21.21	0.056	0.742	-	1.20 / 1.10	8.63	0.4
Ditto	20.21	0.065	0.710	-	1.52 / 0.94	6.63	10.5
InsTaG	26.32	0.026	0.861	3.167	0.93 / 0.31	5.32	82.5

Table 12. **Comparison with DDPM Baselines.** InsTaG shows superior overall performance with real-time inference capability.

6.6. 3D Effect under Extreme Viewing Angles

Here, we visualize the learned 3D heads from 5s data under extreme unseen angles. The results show our learned 3D geometry consistency can be well kept under extreme views, despite some texture degradation due to a lack of data coverage. Notably, the only few training views are mostly frontal, showing our effectiveness and robustness in preserving 3D head structure.



Figure 11. **3D Effect under Extreme Viewing Angles.** Our learned 3D geometry consistency can be well kept under extreme views using only limited data mostly from the front.

7. Dataset Declaration

In the main experiments, all the multimedia data were obtained from existing works [30, 47, 51, 59]. These data were collected from publicly released Internet content. The data used in this work contain only public figures to avoid invading personal privacy. All the data are manually checked to reduce the existence of offensive content.

Specifically, we use 5 ready-made celebrity speaking video clips (named "Obama1", "Jae-in", "Shaheen", "may", "macron") from [33, 59] as the pre-training data, and take the first 5000 frames for each to pre-train the model. To keep fairness, we do not involve videos with an overlapping celebrity in the above pre-training data in evaluation. With such a principle, following the prevailing setting in previous methods [30, 33, 44], we use 4 ready-made videos from [47, 59] as the testing set. To ensure a sound evaluation, we keep at least a clip of 12 seconds for each video for the test in the *self-reconstruction* setting.

In the supplementary video, we also report several models trained with videos collected by ourselves to demonstrate the performance of InsTaG. Since they haven’t been used publicly in previous works or lack a provided preprocessing, we do not involve them in the main experiments, therefore to keep the fairness and soundness.

Diversity of races, genders, ages, and facial features.

We attach great importance to the diversity and try our best to cover different races and genders. However, due to the difficulty in data collection, there are still some lacks. Nevertheless, since our pre-training strategy is identity-free, this negative influence can be weakened.

8. Implementation Details

Preprocessing. Following most previous radiance-field-based works [19, 30, 33], we assume the head to be with a fixed pose in a canonical space and vary the camera pose to represent head rotation. Specifically, we use a BFM [43] model to fit the head pose and inversely get the camera pose for each video frame. An off-the-shelf BiSeNet [63] model is used to segment the head and torso parts and inherit TalkingGaussian [33] to segment the inside mouth and other head areas with EasyPortrait [28]. We represent upper-face expressions with the action units estimated by OpenFace [2, 3]. The audio features are firstly extracted by



Figure 12. **High-definition Comparison.** We shot the generated results from models trained with 5s training data. While other methods produce blurry or distorted regions (yellow box), InsTaG successfully reconstructs a faithful appearance for different identities.

a pre-trained audio encoder like the DeepSpeech [21] used in the main paper, and then reorganized by a trainable CNN attention network from AD-NeRF [19].

Model Architecture. We build the structure field in 3DGS Talking Head Synthesizer based on the 3DGS official implementation¹. The positional encoder of the Universal Motion Field is built with three 2D multi-resolution hash encoders [42], with a resolution range from 16 to 256 and 64 to 384 separately for the face and inside-mouth branches. Then, a 3-layer MLP decoder is behind with hidden dimensions of 64 and 32 for the two branches. In personalized fields, the positional encoder has the same hyperparameter as in UMF, while the dimension of the MLP decoder decreases to 32 and 16. All the 2D hash encoders are set with 12 levels. More details can be found in the source code.

Optimization. Our method inherits the density control strategy of 3DGS to allow the growth of primitives. We start by initializing the radiance field by a random point cloud. In pre-training, we randomly select one frame per iteration from the multi-person data, and calculate the loss to update the model. During adaptation, we first use a small learning rate at the warmup stage with 3000 iterations to build a basic head geometry, and switch on the Motion Aligner in the remaining process.

Baselines. In the main paper, we implement the baselines using their official codes. For the generative models, we use the officially provided weights for reproduction. For all person-specific training, we follow the official instructions to train their models on each video. If available, we uniformly take DeepSpeech [21] as the audio feature extractor for fairness. Specifically, we follow the officially provided scripts to train the model of RAD-NeRF [49], ER-NeRF [30], TalkingGaussian [33] and GaussianTalker [10] with suggested hyperparameters. For GeneFace [59], we select the weight of its fine-tuned landmark predictor following the official instruction based on the losses. For DFRF [47], we fine-tune the models with 50K iterations, which is a bit larger than the 40K iterations provided in its original paper to ensure convergence. For MimicTalk [60], we use the same training video as the fine-tuning data as well as the style reference, and drive the model by the poses from the ground truth.

9. Additional Visualization

In the supplementary materials, we additionally provide high-definition visualized results to show the advantage of InsTaG in visual quality quantitatively. In Figure 12, while

baseline methods generate blurry and distorted details (yellow box) with inadequate training data, InsTaG produces high-fidelity talking heads with a faithful appearance. We additionally provide a [supplementary video](#), which brings a more intuitive and comprehensive comparison.

10. Discussions

Explanation of the design and effect of Negative Contrast Loss. Considering μ decides the global structure of the fields, while s and q are mainly for fitting texture [26], we only include $\Delta\mu$ in the NCLoss. Once the primitive is deformed with two different $\Delta\mu$, it would represent distinct motions even with the same s and q . In our test, adding s and q would not help much.

Why use BFM for head pose estimation? BFM is widely used to estimate head pose in many talking head methods, and it has been inherited by all the NeRF and 3DGS-based baselines in our experiment. For fairness, we also adopt it, although some new models like FLAME perform better. We’ll advance the use of them in future work.

Non-ideal data inputs. Generating high-quality results from non-ideal input is challenging for nearly all methods. By reducing the data demand, our InsTaG makes it easier to capture ideal inputs with a much shorter length. Besides, InsTaG is robust for lower sharpness (first row in Fig. 5) and uneven lighting (two males with side light at video ~08:30). Occlusion or light change may be more challenging. For the former, it may be solved by some in-the-wild techniques. And for the later, adding external light conditions may help. Confidence can also help to filter the low-quality frames. Another way is to leverage the power of generative models to restore the images to a normal one.

11. Ethical Consideration

We propose InsTaG and hope our method can promote the healthy development of digital industries. However, several ethical considerations should be noticed. One key concern pertains to privacy and consent, particularly when training and deploying models on personalized data. To mitigate risks, it is crucial to ensure that all video data in real-world applications should be collected with explicit consent and handled in compliance with data protection regulations.

Another consideration involves the potential misuse of the technology, such as the creation of deceptive deepfakes or unauthorized impersonation. While generative methods are mostly proposed for positive purposes, their capabilities could be exploited for malicious purposes. To address this, safeguards like embedding traceable digital watermarks or partnering with authentication mechanisms can be integrated to distinguish synthetic from real content. We

¹<https://github.com/graphdeco-inria/gaussian-splatting>

will share the results to support the deepfake detection community to help people recognize fake content.

12. Limitation and Future Work

Our proposed InsTaG achieves the fast learning of personalized 3D talking heads from few data, making an advancement in few-shot talking head generation. Nevertheless, some limitations still remain to be addressed in the future.

The first problem is about the extrapolation. Although our pre-training strategy can fetch rich knowledge from existing video data, the basic work principle of the neural fields is still to conduct interpolation between the known signals. Although audio signals can be well generalized by the off-the-shelf audio feature encoder, various upper-face expressions are not easy to be fully covered by the several pre-training data. This would lead to unexpected facial distortion when some unseen expression combinations are input. One of the reasons for this is the instability of the implicit mapping in MLP. We may solve the problem by posing an expression-driving method with a more explicit structure in the future.

Second, the adaptation time of InsTaG is possible to be further shortened. Considering the success of some one-shot 3D head methods, the time of structure reconstruction can be skipped if an accurate 3D head is provided from external. Besides, introducing explicit matching rules may help accelerate the alignment between the pre-trained motion field and the new identity head. We will explore more acceleration techniques in the future.

References

- [1] Alexei Baevski, Yuhao Zhou, Abdelrahman Mohamed, and Michael Auli. wav2vec 2.0: A framework for self-supervised learning of speech representations. *Advances in neural information processing systems*, 33:12449–12460, 2020. 10
- [2] Tadas Baltrušaitis, Marwa Mahmoud, and Peter Robinson. Cross-dataset learning and person-specific normalisation for automatic action unit detection. In *2015 11th IEEE International Conference and Workshops on Automatic Face and Gesture Recognition (FG)*, pages 1–6. IEEE, 2015. 11
- [3] Tadas Baltrušaitis, Amir Zadeh, Yao Chong Lim, and Louis-Philippe Morency. Openface 2.0: Facial behavior analysis toolkit. In *2018 13th IEEE international conference on automatic face & gesture recognition (FG 2018)*, pages 59–66. IEEE, 2018. 11
- [4] James Booth, Epameinondas Antonakos, Stylianos Ploumpis, George Trigeorgis, Yannis Panagakis, and Stefanos Zafeiriou. “3d face morphable models” in-the-wild”. In *Proceedings of the IEEE conference on computer vision and pattern recognition*, pages 48–57, 2017. 3
- [5] Marcel C Bühler, Kripasindhu Sarkar, Tanmay Shah, Gengyan Li, Daoye Wang, Leonhard Helminger, Sergio Orts-Escolano, Dmitry Lagun, Otmar Hilliges, Thabo Beeler, et al. Preface: A data-driven volumetric prior for few-shot ultra high-resolution face synthesis. In *Proceedings of the IEEE/CVF International Conference on Computer Vision*, pages 3402–3413, 2023. 3
- [6] Chen Cao, Tomas Simon, Jin Kyu Kim, Gabe Schwartz, Michael Zollhoefer, Shun-Suke Saito, Stephen Lombardi, Shih-En Wei, Danielle Belko, Shoou-I Yu, et al. Authentic volumetric avatars from a phone scan. *ACM Transactions on Graphics (TOG)*, 41(4):1–19, 2022. 3
- [7] Lele Chen, Zhiheng Li, Ross K Maddox, Zhiyao Duan, and Chenliang Xu. Lip movements generation at a glance. In *Computer Vision—ECCV 2018: 15th European Conference, Munich, Germany, September 8–14, 2018, Proceedings, Part VII 15*, pages 538–553. Springer, 2018. 7
- [8] Lele Chen, Ross K Maddox, Zhiyao Duan, and Chenliang Xu. Hierarchical cross-modal talking face generation with dynamic pixel-wise loss. In *Proceedings of the IEEE/CVF conference on computer vision and pattern recognition*, pages 7832–7841, 2019. 2
- [9] Kai Cheng, Xiaoxiao Long, Kaizhi Yang, Yao Yao, Wei Yin, Yuexin Ma, Wenping Wang, and Xuejin Chen. Gaussianpro: 3d gaussian splatting with progressive propagation. In *Forty-first International Conference on Machine Learning*, 2024. 5
- [10] Kyusun Cho, JoungBin Lee, Heeji Yoon, Yeobin Hong, Jaehoon Ko, Sangjun Ahn, and Seungryong Kim. Gausiantalker: Real-time talking head synthesis with 3d gaussian splatting. In *ACM Multimedia 2024*, 2024. 2, 6, 8, 13
- [11] Joon Son Chung and Andrew Zisserman. Lip reading in the wild. In *Computer Vision—ACCV 2016: 13th Asian Conference on Computer Vision, Taipei, Taiwan, November 20–24, 2016, Revised Selected Papers, Part II 13*, pages 87–103. Springer, 2017. 7
- [12] Joon Son Chung and Andrew Zisserman. Out of time: Automated lip sync in the wild. In *Computer Vision—ACCV 2016 Workshops: ACCV 2016 International Workshops, Taipei, Taiwan, November 20–24, 2016, Revised Selected Papers, Part II 13*, pages 251–263. Springer, 2017. 7
- [13] Paul Ekman and Wallace V. Friesen. *Facial Action Coding System: Manual*. Palo Alto: Consulting Psychologists Press, 1978. 7
- [14] Tony Ezzat, Gadi Geiger, and Tomaso Poggio. Trainable videorealistic speech animation. *ACM Transactions on Graphics (TOG)*, 21(3):388–398, 2002. 2
- [15] Guy Gafni, Justus Thies, Michael Zollhofer, and Matthias Nießner. Dynamic neural radiance fields for monocular 4d facial avatar reconstruction. In *Proceedings of the IEEE/CVF Conference on Computer Vision and Pattern Recognition*, pages 8649–8658, 2021. 3
- [16] Yuan Gan, Zongxin Yang, Xihang Yue, Lingyun Sun, and Yi Yang. Efficient emotional adaptation for audio-driven talking-head generation. In *Proceedings of the IEEE/CVF International Conference on Computer Vision*, pages 22634–22645, 2023. 3, 6, 7
- [17] Baris Gecer, Stylianos Ploumpis, Irene Kotsia, and Stefanos Zafeiriou. Ganfit: Generative adversarial network fitting for high fidelity 3d face reconstruction. In *Proceedings of the IEEE/CVF conference on computer vision and pattern recognition*, pages 1155–1164, 2019. 3

- [18] Simon Giebenhain, Tobias Kirschstein, Markos Georgopoulos, Martin Rünz, Lourdes Agapito, and Matthias Nießner. Monophm: Dynamic head reconstruction from monocular videos. In *Proceedings of the IEEE/CVF Conference on Computer Vision and Pattern Recognition*, pages 10747–10758, 2024. 3
- [19] Yudong Guo, Keyu Chen, Sen Liang, Yong-Jin Liu, Hujun Bao, and Juyong Zhang. Ad-nerf: Audio driven neural radiance fields for talking head synthesis. In *Proceedings of the IEEE/CVF International Conference on Computer Vision*, pages 5784–5794, 2021. 1, 2, 3, 6, 7, 11, 13
- [20] Siddharth Gururani, Arun Mallya, Ting-Chun Wang, Rafael Valle, and Ming-Yu Liu. Space: Speech-driven portrait animation with controllable expression. In *Proceedings of the IEEE/CVF International Conference on Computer Vision*, pages 20914–20923, 2023. 3
- [21] Awni Hannun, Carl Case, Jared Casper, Bryan Catanzaro, Greg Diamos, Erich Elsen, Ryan Prenger, Sanjeev Satheesh, Shubho Sengupta, Adam Coates, et al. Deep speech: Scaling up end-to-end speech recognition. *arXiv preprint arXiv:1412.5567*, 2014. 6, 9, 13
- [22] Yang Hong, Bo Peng, Haiyao Xiao, Ligang Liu, and Juyong Zhang. Headnerf: A real-time nerf-based parametric head model. In *Proceedings of the IEEE/CVF Conference on Computer Vision and Pattern Recognition*, pages 20374–20384, 2022. 3
- [23] Wei-Ning Hsu, Benjamin Bolte, Yao-Hung Hubert Tsai, Kushal Lakhotia, Ruslan Salakhutdinov, and Abdelrahman Mohamed. Hubert: Self-supervised speech representation learning by masked prediction of hidden units. *IEEE/ACM Transactions on Audio, Speech, and Language Processing*, 29:3451–3460, 2021. 10
- [24] Edward J Hu, Phillip Wallis, Zeyuan Allen-Zhu, Yuanzhi Li, Shean Wang, Lu Wang, Weizhu Chen, et al. Lora: Low-rank adaptation of large language models. In *International Conference on Learning Representations*, 2022. 3
- [25] Amir Jamaludin, Joon Son Chung, and Andrew Zisserman. You said that?: Synthesising talking faces from audio. *International Journal of Computer Vision*, 127:1767–1779, 2019. 2
- [26] Bernhard Kerbl, Georgios Kopanas, Thomas Leimkühler, and George Drettakis. 3d gaussian splatting for real-time radiance field rendering. *ACM Transactions on Graphics*, 42(4), 2023. 1, 2, 3, 5
- [27] Rawal Khrodar, Timur Bagautdinov, Julieta Martinez, Su Zhaoen, Austin James, Peter Selednik, Stuart Anderson, and Shunsuke Saito. Sapiens: Foundation for human vision models. In *European Conference on Computer Vision*, pages 206–228. Springer, 2025. 5
- [28] Karina Kvanchiani, Elizaveta Petrova, Karen Efremyan, Alexander Sautin, and Alexander Kapitanov. Easyportrait-face parsing and portrait segmentation dataset. *arXiv preprint arXiv:2304.13509*, 2023. 11
- [29] Dongze Li, Kang Zhao, Wei Wang, Bo Peng, Yingya Zhang, Jing Dong, and Tieniu Tan. Ae-nerf: Audio enhanced neural radiance field for few shot talking head synthesis. In *Proceedings of the AAAI Conference on Artificial Intelligence*, pages 3037–3045, 2024. 3
- [30] Jiahe Li, Jiawei Zhang, Xiao Bai, Jun Zhou, and Lin Gu. Efficient region-aware neural radiance fields for high-fidelity talking portrait synthesis. In *Proceedings of the IEEE/CVF International Conference on Computer Vision*, pages 7568–7578, 2023. 2, 3, 4, 6, 7, 8, 9, 10, 11, 13
- [31] Jiahe Li, Jiawei Zhang, Xiao Bai, Jin Zheng, Xin Ning, Jun Zhou, and Lin Gu. Dngaussian: Optimizing sparse-view 3d gaussian radiance fields with global-local depth normalization. In *Proceedings of the IEEE/CVF Conference on Computer Vision and Pattern Recognition*, pages 20775–20785, 2024. 5
- [32] Jiahe Li, Jiawei Zhang, Xiao Bai, Jin Zheng, Jun Zhou, and Lin Gu. Er-nerf+: Efficient region-aware neural radiance fields for high-fidelity talking portrait synthesis. *Information Fusion*, 110:102456, 2024. 1, 8
- [33] Jiahe Li, Jiawei Zhang, Xiao Bai, Jin Zheng, Xin Ning, Jun Zhou, and Lin Gu. Talkinggaussian: Structure-persistent 3d talking head synthesis via gaussian splatting. In *European Conference on Computer Vision*, pages 127–145. Springer, 2025. 1, 2, 3, 4, 5, 6, 7, 8, 9, 10, 11, 13
- [34] Tianye Li, Timo Bolkart, Michael J. Black, Hao Li, and Javier Romero. Learning a model of facial shape and expression from 4D scans. *ACM Transactions on Graphics, (Proc. SIGGRAPH Asia)*, 36(6):194:1–194:17, 2017. 3
- [35] Tianqi Li, Ruobing Zheng, Minghui Yang, Jingdong Chen, and Ming Yang. Ditto: Motion-space diffusion for controllable realtime talking head synthesis. *arXiv preprint arXiv:2411.19509*, 2024. 11
- [36] Weichuang Li, Longhao Zhang, Dong Wang, Bin Zhao, Zhigang Wang, Mulin Chen, Bang Zhang, Zhongjian Wang, Liefeng Bo, and Xuelong Li. One-shot high-fidelity talking-head synthesis with deformable neural radiance field. In *Proceedings of the IEEE/CVF Conference on Computer Vision and Pattern Recognition*, pages 17969–17978, 2023. 1, 2, 3, 4, 5
- [37] Xian Liu, Yinghao Xu, Qianyi Wu, Hang Zhou, Wayne Wu, and Bolei Zhou. Semantic-aware implicit neural audio-driven video portrait generation. In *Computer Vision—ECCV 2022: 17th European Conference, Tel Aviv, Israel, October 23–27, 2022, Proceedings, Part XXXVII*, pages 106–125. Springer, 2022. 1, 2
- [38] Ilya Loshchilov and Frank Hutter. Decoupled weight decay regularization. In *International Conference on Learning Representations*, 2018. 6
- [39] Yuanxun Lu, Jinxiang Chai, and Xun Cao. Live speech portraits: real-time photorealistic talking-head animation. *ACM Transactions on Graphics (TOG)*, 40(6):1–17, 2021. 2
- [40] Marko Mihajlovic, Aayush Bansal, Michael Zollhoefer, Siyu Tang, and Shunsuke Saito. Keypointnerf: Generalizing image-based volumetric avatars using relative spatial encoding of keypoints. In *European conference on computer vision*, pages 179–197. Springer, 2022. 3
- [41] Ben Mildenhall, Pratul P Srinivasan, Matthew Tancik, Jonathan T Barron, Ravi Ramamoorthi, and Ren Ng. Nerf: Representing scenes as neural radiance fields for view synthesis. In *European Conference on Computer Vision*, pages 405–421. Springer, 2020. 1, 2

- [42] Thomas Müller, Alex Evans, Christoph Schied, and Alexander Keller. Instant neural graphics primitives with a multi-resolution hash encoding. *ACM Transactions on Graphics (ToG)*, 41(4):1–15, 2022. [13](#)
- [43] Pascal Paysan, Reinhard Knothe, Brian Amberg, Sami Romdhani, and Thomas Vetter. A 3d face model for pose and illumination invariant face recognition. In *2009 sixth IEEE international conference on advanced video and signal based surveillance*, pages 296–301. Ieee, 2009. [3](#), [6](#), [11](#)
- [44] Ziqiao Peng, Wentao Hu, Yue Shi, Xiangyu Zhu, Xiaomei Zhang, Hao Zhao, Jun He, Hongyan Liu, and Zhaoxin Fan. Synctalk: The devil is in the synchronization for talking head synthesis. In *Proceedings of the IEEE/CVF Conference on Computer Vision and Pattern Recognition*, pages 666–676, 2024. [2](#), [10](#), [11](#)
- [45] KR Prajwal, Rudrabha Mukhopadhyay, Vinay P Namboodiri, and CV Jawahar. A lip sync expert is all you need for speech to lip generation in the wild. In *Proceedings of the 28th ACM International Conference on Multimedia*, pages 484–492, 2020. [2](#)
- [46] Eduard Ramon, Gil Triginer, Janna Escur, Albert Pumarola, Jaime Garcia, Xavier Giro-i Nieto, and Francesc Moreno-Noguer. H3d-net: Few-shot high-fidelity 3d head reconstruction. In *Proceedings of the IEEE/CVF International Conference on Computer Vision*, pages 5620–5629, 2021. [3](#)
- [47] Shuai Shen, Wanhua Li, Zheng Zhu, Yueqi Duan, Jie Zhou, and Jiwen Lu. Learning dynamic facial radiance fields for few-shot talking head synthesis. In *Computer Vision–ECCV 2022: 17th European Conference, Tel Aviv, Israel, October 23–27, 2022, Proceedings, Part XII*, pages 666–682. Springer, 2022. [1](#), [2](#), [3](#), [4](#), [5](#), [6](#), [7](#), [8](#), [9](#), [11](#), [13](#)
- [48] Luchuan Song, Pinxin Liu, Lele Chen, Guojun Yin, and Chenliang Xu. Tri²-plane: Thinking head avatar via feature pyramid. In *European Conference on Computer Vision*, pages 1–20. Springer, 2025. [3](#)
- [49] Jiaxiang Tang, Kaisiyuan Wang, Hang Zhou, Xiaokang Chen, Dongliang He, Tianshu Hu, Jingtuo Liu, Gang Zeng, and Jingdong Wang. Real-time neural radiance talking portrait synthesis via audio-spatial decomposition. *arXiv preprint arXiv:2211.12368*, 2022. [2](#), [3](#), [6](#), [10](#), [11](#), [13](#)
- [50] Justus Thies, Michael Zollhofer, Marc Stamminger, Christian Theobalt, and Matthias Nießner. Face2face: Real-time face capture and reenactment of rgb videos. In *Proceedings of the IEEE conference on computer vision and pattern recognition*, pages 2387–2395, 2016. [3](#)
- [51] Justus Thies, Mohamed Elgharib, Ayush Tewari, Christian Theobalt, and Matthias Nießner. Neural voice puppetry: Audio-driven facial reenactment. In *Computer Vision–ECCV 2020: 16th European Conference, Glasgow, UK, August 23–28, 2020, Proceedings, Part XVI 16*, pages 716–731. Springer, 2020. [2](#), [7](#), [11](#)
- [52] Kaisiyuan Wang, Qianyi Wu, Linsen Song, Zhuoqian Yang, Wayne Wu, Chen Qian, Ran He, Yu Qiao, and Chen Change Loy. Mead: A large-scale audio-visual dataset for emotional talking-face generation. In *Computer Vision–ECCV 2020: 16th European Conference, Glasgow, UK, August 23–28, 2020, Proceedings, Part XXI*, pages 700–717. Springer, 2020. [2](#)
- [53] Zhou Wang, Alan C Bovik, Hamid R Sheikh, and Eero P Simoncelli. Image quality assessment: From error visibility to structural similarity. *IEEE transactions on image processing*, 13(4):600–612, 2004. [5](#), [7](#)
- [54] Olivia Wiles, A Sophia Koepke, and Andrew Zisserman. X2face: A network for controlling face generation using images, audio, and pose codes. In *Computer Vision–ECCV 2018: 15th European Conference, Munich, Germany, September 8–14, 2018, Proceedings, Part XIII 15*, pages 690–706. Springer, 2018. [2](#)
- [55] Sicheng Xu, Guojun Chen, Yu-Xiao Guo, Jiaolong Yang, Chong Li, Zhenyu Zang, Yizhong Zhang, Xin Tong, and Baining Guo. Vasa-1: Lifelike audio-driven talking faces generated in real time. *arXiv preprint arXiv:2404.10667*, 2024. [3](#)
- [56] Yuelang Xu, Lizhen Wang, Xiaochen Zhao, Hongwen Zhang, and Yebin Liu. Avatarmav: Fast 3d head avatar reconstruction using motion-aware neural voxels. In *ACM SIGGRAPH 2023 Conference Proceedings*, pages 1–10, 2023. [3](#)
- [57] Haotian Yang, Hao Zhu, Yanru Wang, Mingkai Huang, Qiu Shen, Ruigang Yang, and Xun Cao. Facescape: a large-scale high quality 3d face dataset and detailed riggable 3d face prediction. In *Proceedings of the IEEE/cvf conference on computer vision and pattern recognition*, pages 601–610, 2020. [3](#)
- [58] Xihe Yang, Xingyu Chen, Daiheng Gao, Shaohui Wang, Xiaoguang Han, and Baoyuan Wang. Have-fun: Human avatar reconstruction from few-shot unconstrained images. In *Proceedings of the IEEE/CVF Conference on Computer Vision and Pattern Recognition*, pages 742–752, 2024. [3](#)
- [59] Zhenhui Ye, Ziyue Jiang, Yi Ren, Jinglin Liu, Jinzheng He, and Zhou Zhao. Geneface: Generalized and high-fidelity audio-driven 3d talking face synthesis. In *The Eleventh International Conference on Learning Representations*, 2022. [1](#), [2](#), [6](#), [7](#), [8](#), [10](#), [11](#), [13](#)
- [60] Zhenhui Ye, Tianyun Zhong, Yi Ren, Jiaqi Yang, Weichuang Li, Jiangwei Huang, Ziyue Jiang, Jinzheng He, Rongjie Huang, Jinglin Liu, Chen Zhang, Xiang Yin, Zejun Ma, and Zhou Zhao. Mimictalk: Mimicking a personalized and expressive 3d talking face in few minutes. *Advances in neural information processing systems*, 2024. [1](#), [2](#), [3](#), [4](#), [5](#), [6](#), [7](#), [8](#), [13](#)
- [61] Zhenhui Ye, Tianyun Zhong, Yi Ren, Jiaqi Yang, Weichuang Li, Jiawei Huang, Ziyue Jiang, Jinzheng He, Rongjie Huang, Jinglin Liu, et al. Real3d-portrait: One-shot realistic 3d talking portrait synthesis. In *The Twelfth International Conference on Learning Representations*, 2024. [1](#), [2](#), [3](#), [6](#), [7](#)
- [62] Ran Yi, Zipeng Ye, Juyong Zhang, Hujun Bao, and Yong-Jin Liu. Audio-driven talking face video generation with learning-based personalized head pose. *arXiv preprint arXiv:2002.10137*, 2020. [2](#)
- [63] Changqian Yu, Jingbo Wang, Chao Peng, Changxin Gao, Gang Yu, and Nong Sang. Bisenet: Bilateral segmentation network for real-time semantic segmentation. In *Proceedings of the European conference on computer vision (ECCV)*, pages 325–341, 2018. [11](#)

- [64] Hongyun Yu, Zhan Qu, Qihang Yu, Jianchuan Chen, Zhonghua Jiang, Zhiwen Chen, Shengyu Zhang, Jimin Xu, Fei Wu, Chengfei Lv, et al. Gaussiantalker: Speaker-specific talking head synthesis via 3d gaussian splatting. In *Proceedings of the 32nd ACM International Conference on Multimedia*, pages 3548–3557, 2024. [2](#)
- [65] Yu Yu, Kenneth Alberto Funes Mora, and Jean-Marc Odobez. Headfusion: 360° head pose tracking combining 3d morphable model and 3d reconstruction. *IEEE transactions on pattern analysis and machine intelligence*, 40(11): 2653–2667, 2018. [3](#)
- [66] Zhentao Yu, Zixin Yin, Deyu Zhou, Duomin Wang, Finn Wong, and Baoyuan Wang. Talking head generation with probabilistic audio-to-visual diffusion priors. *arXiv preprint arXiv:2212.04248*, 2022. [2](#), [6](#)
- [67] Egor Zakharov, Aliaksandra Shysheya, Egor Burkov, and Victor Lempitsky. Few-shot adversarial learning of realistic neural talking head models. In *Proceedings of the IEEE/CVF international conference on computer vision*, pages 9459–9468, 2019. [3](#)
- [68] Chenxu Zhang, Yifan Zhao, Yifei Huang, Ming Zeng, Saifeng Ni, Madhukar Budagavi, and Xiaohu Guo. Facial: Synthesizing dynamic talking face with implicit attribute learning. In *Proceedings of the IEEE/CVF international conference on computer vision*, pages 3867–3876, 2021. [2](#)
- [69] Richard Zhang, Phillip Isola, Alexei A Efros, Eli Shechtman, and Oliver Wang. The unreasonable effectiveness of deep features as a perceptual metric. In *Proceedings of the IEEE conference on computer vision and pattern recognition*, pages 586–595, 2018. [7](#)
- [70] Longtao Zheng, Yifan Zhang, Hanzhong Guo, Jiachun Pan, Zhenxiong Tan, Jiahao Lu, Chuanxin Tang, Bo An, and Shuicheng Yan. Memo: Memory-guided diffusion for expressive talking video generation. *arXiv preprint arXiv:2412.04448*, 2024. [11](#)
- [71] Hang Zhou, Yasheng Sun, Wayne Wu, Chen Change Loy, Xiaogang Wang, and Ziwei Liu. Pose-controllable talking face generation by implicitly modularized audio-visual representation. In *Proceedings of the IEEE/CVF conference on computer vision and pattern recognition*, pages 4176–4186, 2021. [2](#)